Acta Crystallographica Section D
Biological Crystallography
ISSN 1399-0047

The structure of a deoxygenated 400 kDa haemoglobin reveals ternary- and quaternary-structural changes of giant haemoglobins

Nobutaka Numoto,[a,b,c]‡ Taro Nakagawa,[a,d]§ Ryota Ohara,[a] Tomoyo Hasegawa,[a] Akiko Kita,[c] Takao Yoshida,[e] Tadashi Maruyama,[e] Kiyohiro Imai,[d,f] Yoshihiro Fukumori[a,g]* and Kunio Miki[b]*

[a]Department of Life Science, Graduate School of Natural Science and Technology, Kanazawa University, Kanazawa, Ishikawa 920-1192, Japan, [b]Department of Chemistry, Graduate School of Science, Kyoto University, Sakyo-ku, Kyoto 606-8502, Japan, [c]Research Reactor Institute, Kyoto University, Kumatori, Osaka 590-0494, Japan, [d]Research Center for Micro-Nano Technology, Hosei University, Koganei, Tokyo 184-0003, Japan, [e]Japan Agency for Marine-Earth Science and Technology (JAMSTEC), Yokosuka, Kanagawa 237-0061, Japan, [f]Faculty of Bioscience and Applied Chemistry, Hosei University, Koganei, Tokyo 184-0003, Japan, and [g]School of Natural System, College of Science and Engineering, Kanazawa University, Kanazawa, Ishikawa 920-1192, Japan

‡ Present address: Medical Research Institute, Tokyo Medical and Dental University, 1-5-45 Yushima, Bunkyo-ku, Tokyo 113-8510, Japan
§ Present address: Nagahama Institute of Bio-Science and Technology, Nagahama, Shiga 526-0829, Japan

Correspondence e-mail: fukumor@kenroku.kanazawa-u.ac.jp, miki@kuchem.kyoto-u.ac.jp

Received 25 December 2013
Accepted 14 April 2014

PDB references: V2Hb, oxygenated form, 3wct; deoxygenated form, 3wcu; Ca^{2+}-bound form, 3wcv; Mg^{2+}-bound form, 3wcw

The quaternary structures of invertebrate haemoglobins (Hbs) are quite different from those of vertebrate Hbs. The extracellular giant Hbs of molecular masses of about 400 and 3600 kDa are composed of a dome-shaped dodecameric subassembly which consists of four individual globin subunits. Several crystal structures of 400 kDa Hbs from annelids have been reported, including structures in oxygenated and partially unliganded states, but the structure of the fully deoxygenated state has not been reported. In the present study, crystal structures of V2Hb from the tube worm *Lamellibrachia satsuma* have been determined in both the fully oxygenated and deoxygenated states. A glycosylation site and novel metal-binding sites for divalent cations were clearly observed with no intersubunit interactions in V2Hb. A comparison of the oxygenated and the deoxygenated forms of V2Hb reveals that the ternary- and quaternary-structural changes occur in a manner that maintains the molecular D_3 symmetry. These structures suggest that the mechanisms of quaternary-structural changes between the oxy and deoxy states for the giant Hbs are identical across species.

1. Introduction

Extracellular giant haemoglobins (Hbs) occur in many annelids (Weber & Vinogradov, 2001). Hbs with a molecular mass of about 400 kDa occur in tube worms and beard worms. Another Hb of 3600 kDa (also called erythrocruorin) occurs in earthworms (earthworms and leeches) and sea worms (ragworms, fanworms and tube worms). Tube worms have both the 3600 kDa and the 400 kDa Hbs, which are called V1Hb and V2Hb, respectively. These Hbs share a dodecameric subassembly as a fundamental unit of the giant Hbs (Numoto *et al.*, 2005). The dodecamer is composed of four globin subunits, named A1, A2, B1 and B2, that show a typical globin fold in the manner of myoglobin (Mb). A1 and B1 form a dimer subassembly (A1B1), while A2 and B2 form a similar dimer (A2B2) which is known as the EF-dimer because its interface is constructed by the face-to-face contact of the E and F helices of each subunit (Royer *et al.*, 2001). The EF-dimer structure is widely spread over many invertebrate Hbs, and is quite different from the structure of the $\alpha\beta$ subassembly of the well known mammalian tetrameric Hb. The A1B1 dimer and the A2B2 dimer form a disulfide-bonded tetramer, and three tetramers are assembled into a dome-shaped dodecamer as a fundamental unit of the giant Hbs. The 400 kDa Hbs are composed of two dodecamers that form a hollow spherical structure (Numoto *et al.*, 2005). The oxygen-binding properties of the giant Hbs are distinct from those of vertebrate Hbs (Weber & Vinogradov, 2001; Aki *et al.*, 2007; Fushitani *et al.*, 1986). High oxygen affinity or cooperativity has been reported in some annelid giant Hbs (Weber & Vinogradov, 2001).

Several crystal structures of 400 kDa Hbs have been reported (Numoto *et al.*, 2005, 2008*a*,*b*; Flores *et al.*, 2005), and we have proposed a model of the cooperative mechanism of the 400 kDa Hb based on our recently determined high-resolution structures of the oxygenated and partially unliganded met states of Hb (Numoto *et al.*, 2008*a*,*b*) from the beard worm *Oligobrachia mashikoi*. Because the key residues at the interface of the EF-dimer are highly conserved among the giant Hbs of annelids, the cooperative mechanism of the EF-dimer is expected to be shared among all giant Hbs of this phylum. However, since no crystal structure of the ferrous deoxygenated state of the giant Hbs has been reported, there is room for discussion about the more precise structural basis of the allosteric transition based on the fully oxygenated and deoxygenated structures of the giant Hbs.

Here, we report the crystal structures of a 400 kDa Hb (V2Hb) from the tube worm *Lamellibrachia satsuma* in both the fully oxygenated and deoxygenated states. The structures reveal the glycosylation site, which is not observed in other giant Hbs. In addition, the Ca^{2+}- and Mg^{2+}-binding sites of V2Hb are quite different from those of another previously reported 400 kDa Hb. A comparison between the oxy and deoxy forms shows the ternary and quaternary changes that appear to be made in order to maintain the molecular twofold and threefold symmetry.

2. Materials and methods

2.1. Tube-worm collection

The tube worm *L. satsuma* was collected several times from the colonies on the shallow mud seabed of the 'Tagiri' vents bubbling volcanic gases (mainly CO_2, H_2S and N_2) at a depth of about 95 m in the innermost bay area of Kagoshima Bay (31° 39′ N, 130° 48′ E) by the dredging operation of the training ship Nansei-maru of Kagoshima University or by the remotely operated vehicle Hyper-Dolphin associated with the research vessel Natsushima of the Japan Agency for Marine-Earth Science and Technology (JAMSTEC). The collected tube worms were quickly washed and kept in fresh seawater in a large container on board. After returning to Kagoshima port, the live worms were quickly transported to a laboratory at Kagoshima University, Kagoshima City Aquarium 'Io World', Kanazawa University or JAMSTEC.

2.2. Blood sampling

The bodies of live worms were cut and laid on a metallic mesh filter, and the blood that passed through the filter was collected into a beaker on ice. The blood was centrifuged for 30 min at 10 000*g* and 4°C. The bright red supernatant containing the giant Hbs was quickly frozen in a cryotube with liquid nitrogen and kept in a liquid-nitrogen container or a deep freeze until use.

2.3. Giant Hb purification

The frozen blood in the cryotube was rapidly thawed using running tap water and concentrated at 4°C by ultrafiltration with an Amicon Ultra-15 100 K cutoff filter (Millipore) using a high-speed centrifuge. The purification experiments were conducted in a cold room. The concentrated sample was applied onto a Sephacryl S-400 gel-filtration column (2.6 cm diameter × 100 cm; GE Healthcare) equilibrated with the buffer 50 m*M* Tris–HCl pH 8.0, 200 m*M* NaCl, 50 m*M* $CaCl_2$, 50 m*M* $MgCl_2$ and the chromatography was performed at a flow rate of 0.4 ml min^{-1}. The absorbances of 2 ml aliquots of each fraction were analyzed at both 416 and 280 nm using a UV-265FS spectrophotometer (Shimadzu Co., Kyoto, Japan). Two main peaks corresponding to ∼3600 kDa V1Hb and 440 kDa V2Hb appeared and showed a constant ratio of absorbance at 416 and 280 nm: 2.4 for V1Hb and 2.8 for V2Hb. Both of the Hb fractions were concentrated by ultrafiltration and exchanged into a suitable buffer for the subsequent experimental conditions by dialysis. The giant Hbs obtained were used in the experiments without freezing as soon as possible to maintain the native Hb structure in the oxygenated state.

2.4. Electrophoresis analyses

The V2Hb sample was lysed in Laemmli sample buffer under reduced conditions with β-mercaptoethanol (Laemmli, 1970) and boiled for 5 min. SDS–polyacrylamide gel (18% T, 3% C) containing 6 *M* urea without glycerol was electrophoresed at a constant current of 35 mA using a tricine SDS–PAGE system (Schägger & von Jagow, 1987). After electrophoresis, the gel was stained for 20 min with Coomassie Brilliant Blue (CBB) staining solution and decolourized with deionized water or destaining solution. Two protein bands for the B1 subunit were located at ∼18 kDa, but the other subunits around the typical globin size of ∼16 kDa overlapped with each other to form a large band.

2.5. N-terminal amino-acid sequencing

After SDS–PAGE, the protein bands of V2Hb were electrotransferred to a PVDF membrane using a semi-dry blotting system at a constant current of 1 mA cm^{-2} for 2 h with different transfer buffers: the cathode buffer consisted of 10 m*M* CAPS–NaOH pH 11.0, 10% methanol and the anode buffer was this buffer containing 0.1% SDS. The blotted membrane was stained using a CBB staining solution consisting of 0.1% CBB, 42% methanol, 16% acetic acid and was destained using 40% methanol. The five bands from V2Hb on the membrane were carefully cut and destained using 100% methanol.

The N-terminal 20 amino acids of each of these bands were determined by the method of Edman degradation and HPLC separation with an ABI Model 476A Protein Sequencer (Applied Biosystems, USA), although cysteine residues could not be detected. The resultant 20-amino-acid sequences of the five bands of V2Hb were as follows: A1, (D/S)-T-N-(I/G)-L-Q-R-L-K-V-K-M-Q-W-A-K-A-Y-G-F; A2, (S/D)-E-T-(G/I)-P-L-Q-R-L-K-V-K-M-Q-W-A-E-A-Y-G; B1, S-E-F-T-S-E-A-D-A-T-I-V-I-K-Q-W-N-Q-I-Y; B2, (S/D)-(S/E)-N-(G/I)-(P/L)-(T/L)-(T/E)-(E/L)-(D/L)-K-V-(E/V)-(E/Q)-(Q/F)-(L/A)-(A/K)-(W/A/E)-(A/Y)-(N/Y)-(V/G). The unclear result for the B2

Table 1
Data-collection and refinement statistics.

Values in parentheses are for the highest resolution shell.

	Oxy	Deoxy	50 m*M* Ca^{2+}	50 m*M* Mg^{2+}
Data collection				
Wavelength (Å)	0.9000	0.9000	1.0000	1.0000
Space group	$P6_3$	$P6_3$	$P6_3$	$P6_3$
Unit-cell parameters (Å)				
a	108.56	108.87	108.94	109.27
c	193.55	195.16	195.02	195.60
Resolution (Å)	50–2.40 (2.49–2.40)	50–2.90 (3.00–2.90)	50–2.60 (2.69–2.60)	50–2.50 (2.59–2.50)
No. of observations	589213	160754	230481	259924
No. of unique reflections	50516	28054	40209	45675
Completeness (%)	100 (100)	96.5 (98.8)	99.9 (100)	99.9 (100)
Average $I/\sigma(I)$	28.6 (6.7)	13.2 (4.2)	22.9 (5.1)	15.1 (4.0)
Multiplicity	11.7 (11.7)	5.7 (5.6)	5.7 (5.6)	5.7 (5.8)
R_{merge} (%)†	8.6 (42.3)	9.6 (50.3)	6.5 (33.7)	10.4 (39.5)
Refinement				
R‡ (%)	21.6	24.6	23.5	20.7
R_{free}§ (%)	26.4	29.2	26.7	25.9
No. of atoms				
Protein	9108	4569	9117	9108
Haem and oxygen	360	172	360	360
Carbohydrate	142	71	142	142
Ca^{2+}	2	1	6	0
Mg^{2+}	0	0	0	3
Water	152	0	59	212
Average *B* factor (Å^2)	48.1	70.8	61.7	42.0
R.m.s. deviation from ideal				
Bond lengths (Å)	0.007	0.009	0.010	0.008
Angles (°)	1.1	1.2	1.3	1.2
Ramachandran plot (%)				
Favoured region	97.0	88.2	96.1	95.9
Allowed region	2.8	11.6	3.5	3.8
Outlier region	0.2	0.2	0.4	0.3

† $R_{merge} = \sum_{hkl}\sum_i |I_i(hkl) - \langle I(hkl)\rangle| / \sum_{hkl}\sum_i I_i(hkl)$, where $\langle I(hkl)\rangle$ is the mean intensity after rejection. ‡ $R = \sum_{hkl} ||F_{obs}| - |F_{calc}|| / \sum_{hkl} |F_{obs}|$, where F_{obs} is the observed structure-factor amplitude and F_{calc} is the calculated structure-factor amplitude. § R_{free} is the same as R but calculated using a random set containing 5% of the data that were excluded during refinement.

band is owing to contamination with A2 since the bands overlapped on the SDS–PAGE gel. The A1 and A2 bands also overlapped to a lesser degree.

2.6. cDNA analyses

The tube-worm body was extruded from the worm's chitinous tube by injection of fresh seawater with a syringe and stored in a deep-freeze on board the ship. Trophosome tissue was dissected from a body preserved at −80°C and total RNA was extracted using TRIzol (Invitrogen, Carlsbad, California, USA) according to the manufacturer's instructions. Poly-(A)+ RNA was then purified from the total RNA using an Oligotex-dT30 Super mRNA Purification Kit (Takara Bio Inc., Shiga, Japan) and a cDNA library was generated using a cDNA Synthesis Kit (Takara Bio Inc.) with an oligo(dT) primer, 5′-$(GA)_{10}$ACTAGTCTCGAG$(T)_{18}$V-3′, according to the manufacturer's instructions. After cDNA synthesis, the cDNAs were blunted and ligated to an *Eco*RI adapter: 5′-AATTCGGCACGAGG-3′. They were digested with *Xho*I and *Eco*RI and ligated to a pBluescript II SK (+) vector (Stratagene, La Jolla, California, USA). *Escherichia coli* strain DH10B was transformed with the constructed cDNA library by electroporation. 5′-Terminal sequencing of the cDNA library was performed using a DYEnamic ET dye terminator kit (GE Healthcare, Buckinghamshire, England) with an RV-M primer, 5′-GAGCGGATAACAATTT-CACACAGG-3′, on a MegaBASE4000 (GE Healthcare). The obtained raw sequence chromatogram files were base-called using the *Phred* software (Ewing *et al.*, 1998). The sequences with a Phred quality value of less than 15 and vector/adapter sequences were eliminated by *PFP* (*Paracel Filtering Package*; Paracel). The resultant sequences were assembled using the *CAP*4 assembler v.2.6.2. Similarity searches for all expressed sequence tags (ESTs) obtained were conducted for all databases using *BLAST* on the NCBI site (http://blast.ncbi.nlm.nih.gov/Blast.cgi). The 20 ESTs of four subunits of V2Hb were identified on the basis of each determined N-terminal amino-acid sequence and the high homology of the globin chains of the giant Hbs from related annelids.

2.7. Crystallization, data collection, model building and refinement

Oxygenated crystals were obtained by the sitting-drop vapour-diffusion method at 20°C using equal volumes of protein solution and reservoir solution consisting of 13–18%(*w*/*v*) polyethylene glycol (PEG) 3350, 100 m*M* HEPES–NaOH pH 7.5, 0–5 m*M* calcium acetate or magnesium acetate. Crystals appeared within two weeks and grew to maximum dimensions of 0.3 × 0.3 × 0.6 mm within 3–4 weeks.

Prior to data collection, the oxy crystals were soaked in a solution consisting of 100 m*M* HEPES–NaOH pH 7.5, 16%(*w*/*v*) PEG 3350, 0–50 m*M* $CaCl_2$ or $MgCl_2$, 20%(*v*/*v*) PEG 400. The crystals were transferred into solutions increasing to a final concentration of 20%(*v*/*v*) PEG 400 in a stepwise manner and flash-cooled under a nitrogen-gas stream at −183°C.

The deoxy crystals were obtained from the oxy crystals using a soaking method in almost in the same way as described above, but in the last step the crystals were soaked in a cryoprotectant solution containing 50 m*M* sodium hydrosulfite and incubated for typically 5 min. The crystals then were immediately flash-cooled under a nitrogen-gas stream at −183°C.

X-ray diffraction experiments were performed on beamlines BL41XU and BL44XU at SPring-8. The data were processed and scaled using the *HKL*-2000 package (Otwinowski & Minor, 1997) and were truncated using the *CCP*4

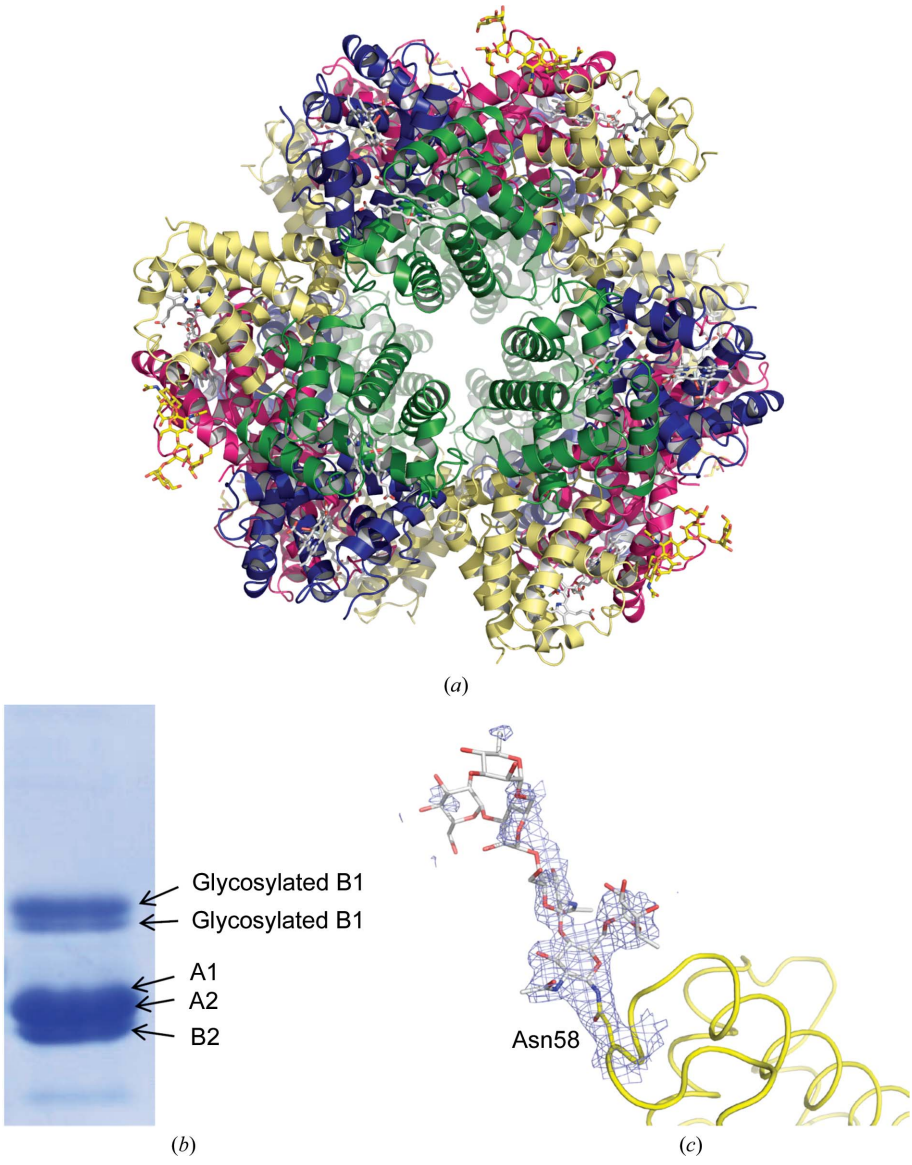

Figure 1
(*a*) Overall structure of V2Hb. The globin subunits A1, A2, B1 and B2 are shown in red, green, yellow and blue, respectively. The carbohydrate chains at the B1 subunits are drawn as stick models. (*b*) SDS–PAGE analysis (18% acrylamide gel containing 6 *M* urea) V2Hb. The A1, A2 and B2 subunits appear as a large band because of their close molecular masses of ∼16 kDa. Double bands of the glycosylated B1 subunit also appear on top of them. (*c*) Electron-density maps contoured at the 0.8σ level and the model for the carbohydrate chains including Asn58 of the B1 subunit are shown as a blue mesh and a stick model, respectively. The protein molecule (B1) is indicated as a yellow loop.

program suite (Winn *et al.*, 2011). For further refinement, 5% of the reflections were set apart as a random test set to calculate the $R_{\rm free}$ value.

The structure of the 400 kDa coelomic Hb from *Riftia pachyptila* (PDB entry 1yhu; Flores *et al.*, 2005) was used as a search model for molecular replacement using *MOLREP* (Vagin & Teplyakov, 2010). Several cycles of manual model rebuilding and refinement were performed using *Coot* (Emsley *et al.*, 2010) and *CNS* (Brünger *et al.*, 1998), respectively. After each cycle, $2F_{\rm o} - F_{\rm c}$ and $F_{\rm o} - F_{\rm c}$ electron-density maps were calculated to check the fit of the model to the maps. Solvent molecules were placed by identification of peaks greater than 3σ in the $F_{\rm o} - F_{\rm c}$ map and with geometries suitable for hydrogen bonding. For the deoxy structure, the model was constructed of only one copy of each of the four subunits and was refined by applying strict NCS constraints. The statistics of data collection and refinement are summarized in Table 1. The figures were prepared with *PyMOL* (http://www.pymol.org/).

3. Results and discussion

3.1. Oxygenated form of V2Hb

Lamellibrachia V2Hb in both the oxygenated and deoxygenated states consists of six copies of four globin subunits (A1, A2, B1 and B2) and forms a hollow spherical structure with 32 molecular symmetry (Fig. 1*a*). The molecular architecture of V2Hb is the same as those of *Oligobrachia* Hb (Numoto *et al.*, 2005, 2008*b*) and the coelomic Hb from the tube worm *R. pachyptila* (*Riftia* C1; Flores *et al.*, 2005). The oxy and deoxy crystals of V2Hb belonged to space group $P6_3$ and the asymmetric unit contained two copies of each of the four subunits (*i.e.* one third of one V2Hb molecule). A superposition of the oxy structure of V2Hb with the structures of oxygenated *Oligobrachia* Hb and CO-bound *Riftia* C1 showed r.m.s.d. values of 2.7 Å (3240 C^{α} atoms) and 2.1 Å (3498 C^{α} atoms), respectively. Sequence alignments (Supplementary Fig. S1[1]) among the giant Hbs for which crystal structures are known show that the amino-acid sequence of each of the four subunits of V2Hb reveals the highest similarity to those of *Riftia* C1. Both V2Hb and *Riftia* C1 lack the inter-subunit disulfide bonds at the N-terminal side between the B1 and B2 subunits, yet these Hbs maintain the dodecameric subassembly.

The amino-acid sequence of the B1 subunit contains a potential N-linked glycosylation site (Asn-*X*-Ser/Thr) at Asn58 which is specifically recognized and catalyzed by the oligosaccharyltransferase complex on the endoplasmic reticulum lumen. SDS–PAGE analysis showed that two bands corresponding to B1 subunits appeared to migrate to higher positions than the other strong bands corresponding to A1, A2

[1] Supporting information has been deposited in the IUCr electronic archive (Reference: YT5066).

and B2 subunits around ∼16 kDa, which is the typical globin size (Fig. 1*b*), suggesting that the B1 subunit was modified by carbohydrate chains. Moreover, only two bands of ∼18 kDa B1 subunits were clearly stained using the glycoprotein staining method, suggesting that two types of carbohydrate chains are present in the B1 subunits of V2Hb (data not shown). Indeed, significant electron densities that were thought to correspond to a carbohydrate chain are observed at the Asn58 residue of all B1 subunits. The electron density of the oligosaccharide moiety indicates that the sugar chain showed a typical high-mannose pattern, but the well defined electron density of the Asn-linked *N*-acetylglucosamine (NAG) clearly exhibited features of fucosylation (Fig. 1*c*). The carbohydrate chain at the B1 subunit is directed towards the outside of the spherical molecule of V2Hb, and there are no intramolecular contacts between the oligosaccharide and protein moieties. Thus, it remains unclear whether the sugar chain could act on the stabilizing and functional mechanisms of V2Hb, while the local dynamics of the glycosylation site, located in a loop region just before the E helix, might be reduced (discussed below).

Strong electron densities (maximum value of 6.0σ) that can be interpreted as Ca^{2+} ions are found between the G and H helices of the A2 subunits in both the oxy and deoxy structures. This site is quite different from the case of *Oligobrachia* Hb, in which three identical Ca^{2+} binding sites are located at the interfaces of the globin subunits (Numoto *et al.*, 2008*b*). The side chains of Asn106, Glu109 and Asp135 of V2Hb contribute to this metal-binding site along with three solvent molecules (site 1; Fig. 2*a*). In the case of the oxy structure, the crystal was obtained from crystallization drops containing 5 m*M* Ca^{2+} ion. The peak densities of site 1 are 5.4σ and 6.0σ, and the Ca^{2+} ions are coordinated by the above three residues and three waters, forming a heptacoordination. The Ca^{2+} binding sites are located on the surface of the molecule, and no intersubunit interactions are observed. To identify other candidates for Ca^{2+} binding sites, we performed crystallization at higher concentrations (100–160 m*M*) of Ca^{2+} ions.

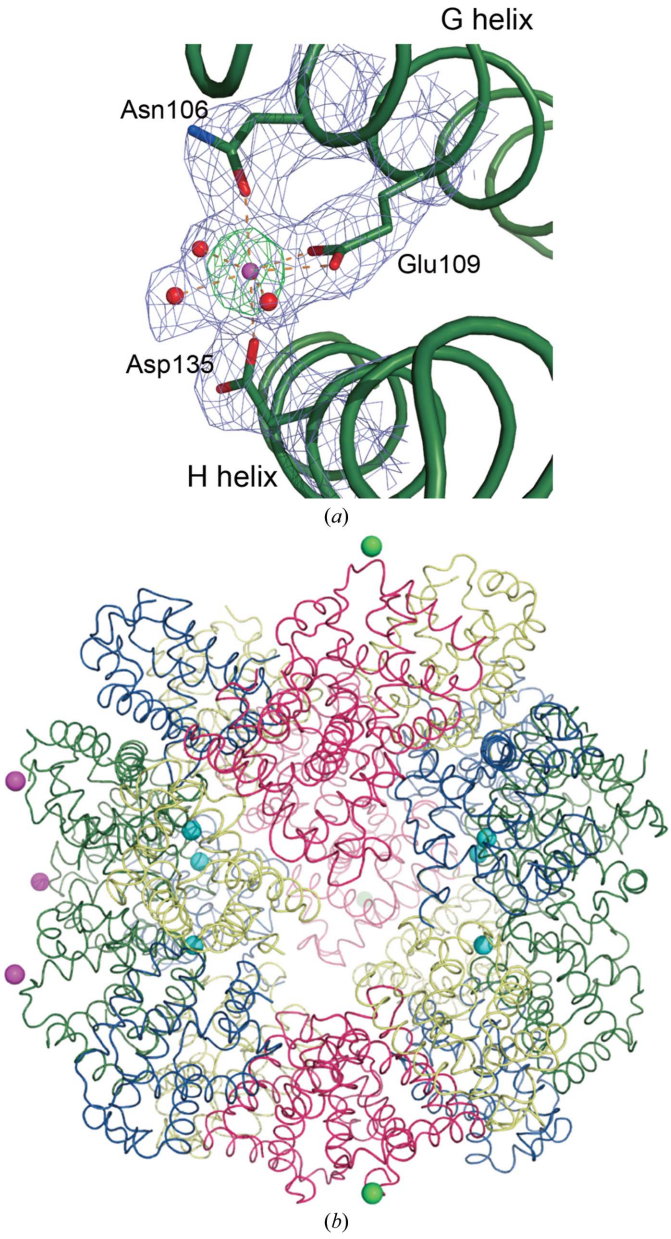

Figure 2
(*a*) Close-up view of the major Ca^{2+} ion (magenta) binding site in the A2 subunit. The $2F_o - F_c$ map (cyan, 1.2σ) and metal-omitted $F_o - F_c$ map (green, 8.0σ) are represented. Dashed lines indicate the coordination geometry of the Ca^{2+} ion. (*b*) The positions of the minor metal-binding sites (sites 2, 3 and 4) are indicated in the whole molecule of V2Hb. The Ca^{2+} ions in sites 2 and 3 are shown in magenta and cyan, respectively. The Ca^{2+} or Mg^{2+} ions in site 4 are shown in green.

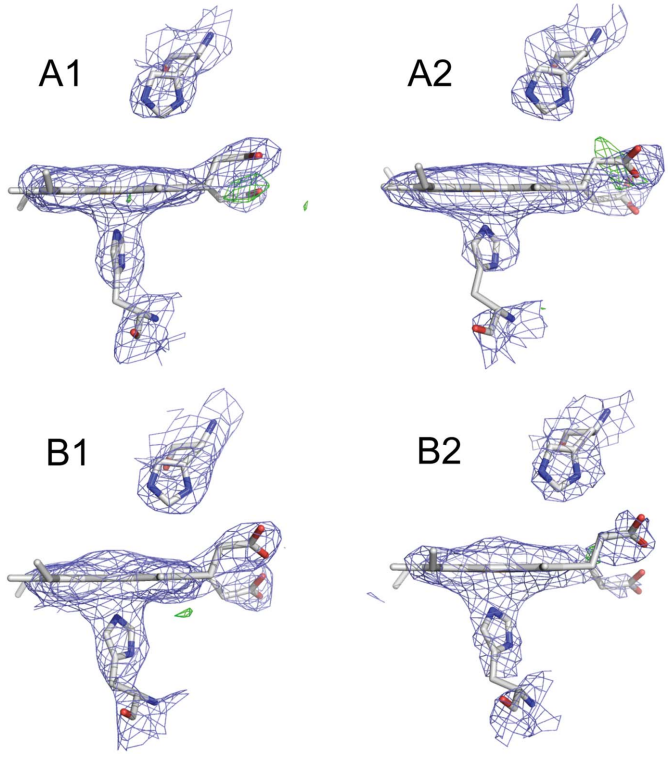

Figure 3
The $2F_o - F_c$ maps (cyan, contoured at 1.2σ) and the ligand-omitted $F_o - F_c$ maps (green, contoured at 3.0σ; red, contoured at −3.0σ) around the ligand sites at all four subunits in the deoxy form.

However, we obtained an unusual diffraction pattern from the crystals obtained under higher salt conditions (Supplementary Fig. S2*a*). Broad twofold peaks in the self-rotation function and strong non-origin Patterson peaks (Supplementary Figs. S2*b* and 2*c*) suggested that these observations were probably caused by lattice-translocation defects (Wang *et al.*, 2005). To avoid these crystallization problems, we crystallized V2Hb under lower salt conditions and then soaked the crystals in higher concentrations of salts. The crystal soaked in a solution containing 50 m*M* Ca^{2+} revealed other Ca^{2+} binding sites which are located near Gly99 and Glu119 of the A2 subunit and Asp95 of the A1 subunit (sites 2, 3 and 4, respectively; Fig. 2*b*). Both sites 2 and 4 are also located on the surface of the molecule, and the bound Ca^{2+} contacts the neighbouring molecule by crystal packing. Site 3 is located within the hollow cavity of the molecule. No intersubunit interactions are observed among all these Ca^{2+} binding sites in the V2Hb molecule. Moreover, the electron density of the crystal grown under the condition 5 m*M* Mg^{2+} and soaked in a solution containing 50 m*M* Mg^{2+} before data collection shows weak and strong peaks for metal ions. These sites are identical to sites 1 and 4 of the Ca^{2+} bound form, respectively (Fig. 2*b*). A preliminary study on the oxygenation properties of V2Hb in the absence or presence of divalent cations confirmed that the addition of Mg^{2+} and Ca^{2+} ions resulted in few changes in the oxygenation properties of V2Hb (data not shown). We conclude that the metal ions in site 1 would contribute to extra structural stability by bridging between the G and H helices. The peaks for site 1 were clearly observed even when the crystal was obtained in the condition containing 5 m*M* Ca^{2+}, which is consistent with the concentration in seawater.

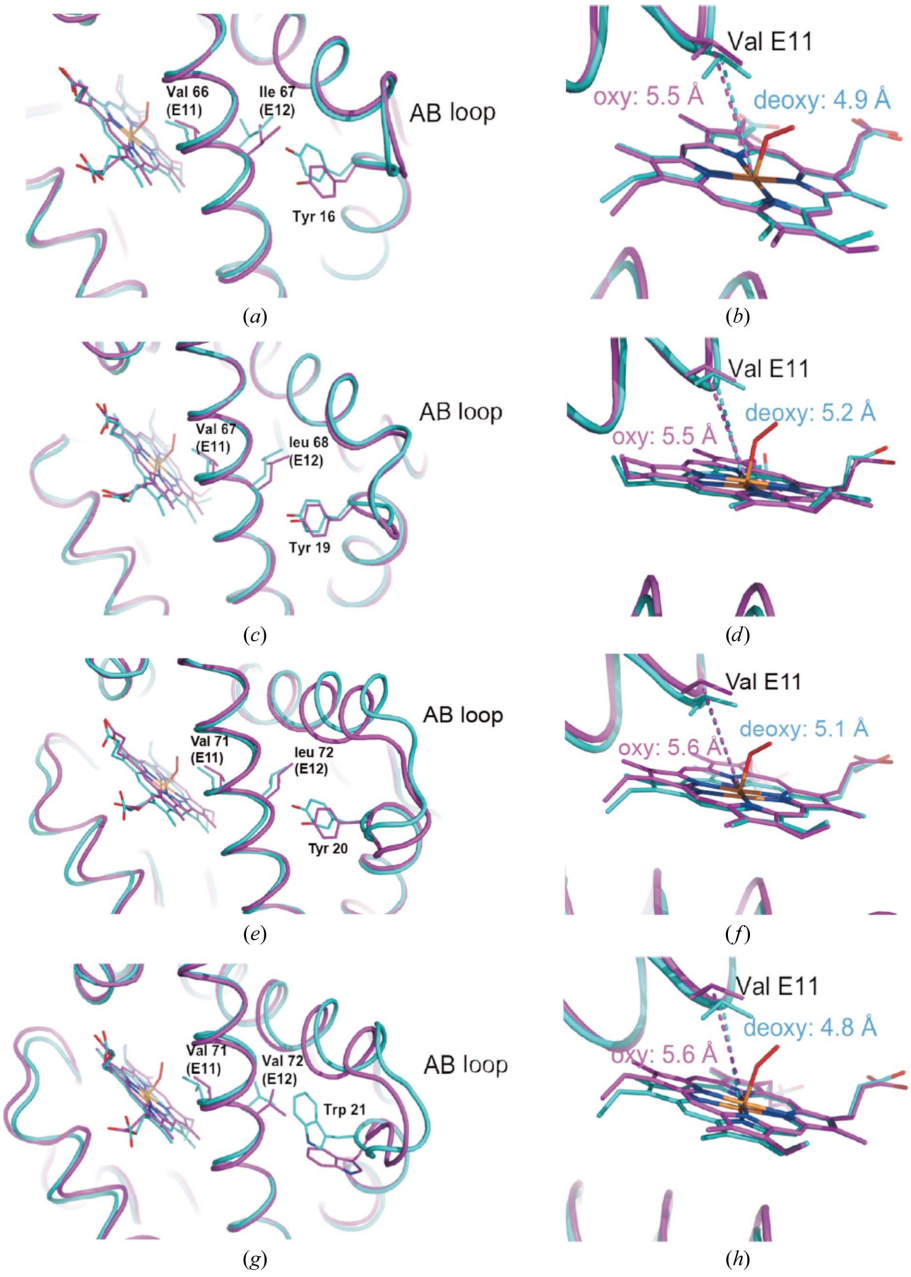

Figure 4
Comparisons of each subunit of oxygenated (magenta) and deoxygenated (cyan) V2Hb. The AB loop region and neighbouring E helix move complementarily owing to the bulky residue, and E11 and E12 are shown as stick models in (*a*), (*c*), (*e*) and (*g*) corresponding to the A1, A2, B1 and B2 subunits, respectively. (*b*), (*d*), (*f*) and (*h*) are close-up views around the ligand-binding pockets of the A1, A2, B1 and B2 subunits, respectively. Distances between the haem iron and Val E11 C^{β} atoms are indicated (dashed line). Note that the haem structures in deoxy V2Hb were refined with tight restraints to maintain a planar conformation of the porphyrin moiety.

3.2. Deoxygenated form of V2Hb

The oxygenated crystals were soaked in a solution containing 50 m*M* sodium hydrosulfite, and the colour of the crystals gradually turned from bright red to dark red within 1–2 min. This indicates that the oxygenated state of the crystals becomes the deoxygenated form. The soaking time was set to be no longer than 5 min to obtain fully deoxygenated and satisfactorily diffracting crystals, because a long soaking treatment resulted in poor diffraction, possibly owing to a shift in the solubility on addition of the cryoprotectant.

In the deoxy crystal, no significant peaks for any ligand molecules were observed in the electron-density ($2F_o - F_c$ and $F_o - F_c$) maps around the distal side of the haems (Fig. 3). This fact strongly suggests that the obtained structure was a fully deoxygenated form. In addition, the absorption spectra of the V2Hb solution mixed with the same solution used to make the deoxy crystals showed a spectral pattern

similar to that for deoxygenated Hb reported elsewhere (Supplementary Fig. S3). Based on the above facts, we concluded that the obtained structure was the fully deoxygenated form of V2Hb.

3.3. Ternary-structural changes between the oxy and deoxy V2Hb

A comparison between the oxy and deoxy forms of V2Hb reveals ternary-structural changes in all subunits (Fig. 4). The most significant changes are observed in the AB loop region of each subunit. The AB loop moves towards the E helix, which contains the distal His and other residues around the haem pockets in the deoxy form. A bulky residue such as Tyr or Trp is located at the end of the AB loop or the beginning of the B helix in each subunit, and the conformations of all of these residues are shifted toward the E helix, causing the helix structure to bend at the side chain of Val E11 (Figs. 4*a*, 4*c*, 4*e* and 4*g*). The E-helix bending of each subunit in the deoxy form results in the protrusion of Val E11 towards the ligand-binding site (Figs. 4*b*, 4*d*, 4*f* and 4*h*) and would thereby cause a reduction in the oxygen-binding affinity because of its steric hindrance.

The ternary-structural changes around Val E11 coupled with the conformational changes of the bulky residues in the AB loop are commonly seen in all subunits of both V2Hb and *Oligobrachia* Hb (Numoto *et al.*, 2008*a*). A similar ternary-structural change is also observed in the β subunit of human HbA. It is known that Val E11 in the β subunit protrudes toward a ligand-binding pocket in the deoxy state, and these changes are coupled to the conformational changes around the AB loop region, especially the shift at Val20 towards the E helix (Supplementary Fig. S4*a*). In contrast, structural changes around Val E11 of the α subunit of HbA are scarcely observed between the oxy and deoxy forms, although slight conformational changes at the AB loop are observed. It is noteworthy, on the other hand, that Trp14 of the α subunit flips outside the molecule in the oxy form and two molecules of toluene are located in the cleft between the E helix and the AB loop (Supplementary Fig. S4*b*). Since it has been reported that the preparation of crystals of oxygenated HbA requires toluene as an additive reagent (Perutz, 1968), hydrophobic molecules (or residues) are thought to be necessary for stabilizing the oxy state at the cleft between the E helix and the AB loop. These facts may suggest that Val E11 of the α subunit is more flexible and unstable in the absence of toluene. Thus, these findings raise the possibility that the ternary-structural changes around Val E11 coupled with the AB loop are a common property of some Hbs to modify the oxygen binding in different species.

3.4. Quaternary-structural changes between oxy and deoxy V2Hb

Quaternary-structural rearrangements of V2Hb between the oxy and deoxy forms are also observed. A superposition of the A1B1 dimers of both the oxy and deoxy forms performed by the fitting of each A1 subunit reveals that deoxy V2Hb shows a tighter conformation than that of oxy V2Hb (Supplementary Fig. S5). At the interface of the dimer, the conformational changes around the A1 haem lead to a sliding movement of the F helix of the neighbouring B1 subunit, and this rearrangement causes environmental changes of the haem pocket of the B1 subunit (Fig. 5*a*). The sliding movement of the B1 F helix results in conformational changes of the haem and Val E11 of the B1 subunit, as discussed above. The same quaternary-structural rearrangements are observed at the interface of the A2B2 dimer (Fig. 5*b*). Therefore, the dimeric subassemblies are primarily responsible for the cooperative oxygen binding of V2Hb.

The quaternary-structural changes throughout a whole molecule of V2Hb occur in a manner that maintains the molecular symmetry. Relatively small quaternary-structural changes are observed around the molecular twofold and threefold axes, whereas large movements are seen at the edge of the spherical 24-mer molecule (Supplementary Movie). The

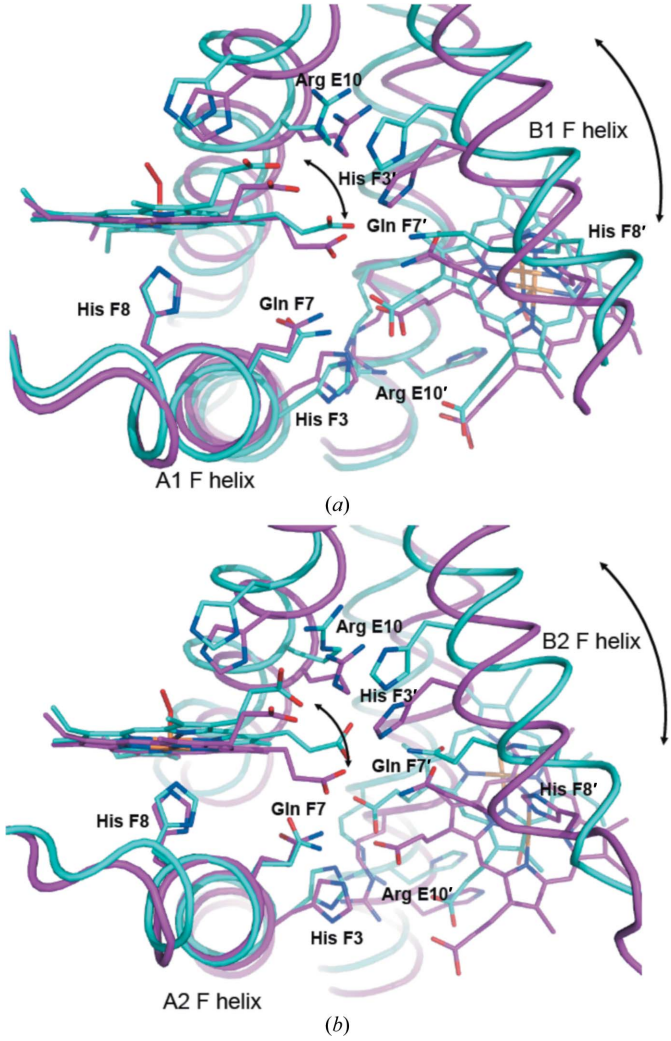

Figure 5
Structural changes around the interface of the dimer subassemblies of V2Hb. Structures of deoxy V2Hb are superimposed onto those of oxy V2Hb by fitting of the proximal His (F8) of the A1 subunit (*a*) and the E helices of the A2 subunits (*b*). Residues marked with a prime belong to the B1 or B2 subunits. Arrows indicate the relative scales of the structural changes around the interfaces.

end of the B helix (Lys38 and Val39) and the middle part of the G helix (His110) of the A2 subunit are closest to the threefold axis. The distances of the corresponding C^{α} atoms around these regions are about 0.2 Å between the oxy and deoxy structures, whereas movements of about 1.3 Å are observed for the AB loop (Tyr19) and the F helix (Ser93), which are far from the molecular threefold axis (Fig. 6). At the twofold axis, the latter part of the G helix (Val115) of the A1 subunit is located just beside the symmetry axis, and moves only 0.17 Å from the deoxy to the oxy form. On the other hand, the AB loop (Phe20) and the middle part of the E helix (Ile67) move more than 1 Å at the outside of the twofold axis. In the B1 and B2 subunits, the former parts of the A helices move small distances of 0.23 and 0.08 Å at B1 Ala7 and B2 Asp9, respectively, because both N-termini are near the twofold axis. Owing to the disulfide bonds between the N-termini and the H helices, the former parts of the H helices of the B1 and B2 subunits also show only a slight movement of about 0.2–0.3 Å. In contrast, movements of more than 1.5 Å occur around the AB loops and the end of the F helices, which are located far from the twofold axis.

We have reported the structures of *Oligobrachia* Hb in the oxy and partially unliganded met states, and we found that the partially unliganded met state of *Oligobrachia* Hb forms a nearly T-state (unliganded) rather than R-state (liganded) structure, contrary to the case in vertebrate Hbs (Numoto *et al.*, 2008*a*,*b*). The quaternary changes of *Oligobrachia* Hb are quite similar to those of V2Hb discussed above, although the 'partially unliganded met state' is not equivalent to the 'fully deoxygenated state'. The distances of the corresponding C^{α} atoms between the oxy and met(A1-oxy) states of *Oligobrachia* Hb are well matched to those in V2Hb, with several exceptions (Fig. 6). In the A2 subunit, large distances at the GH loop region are observed in *Oligobrachia* Hb. The Ca^{2+}

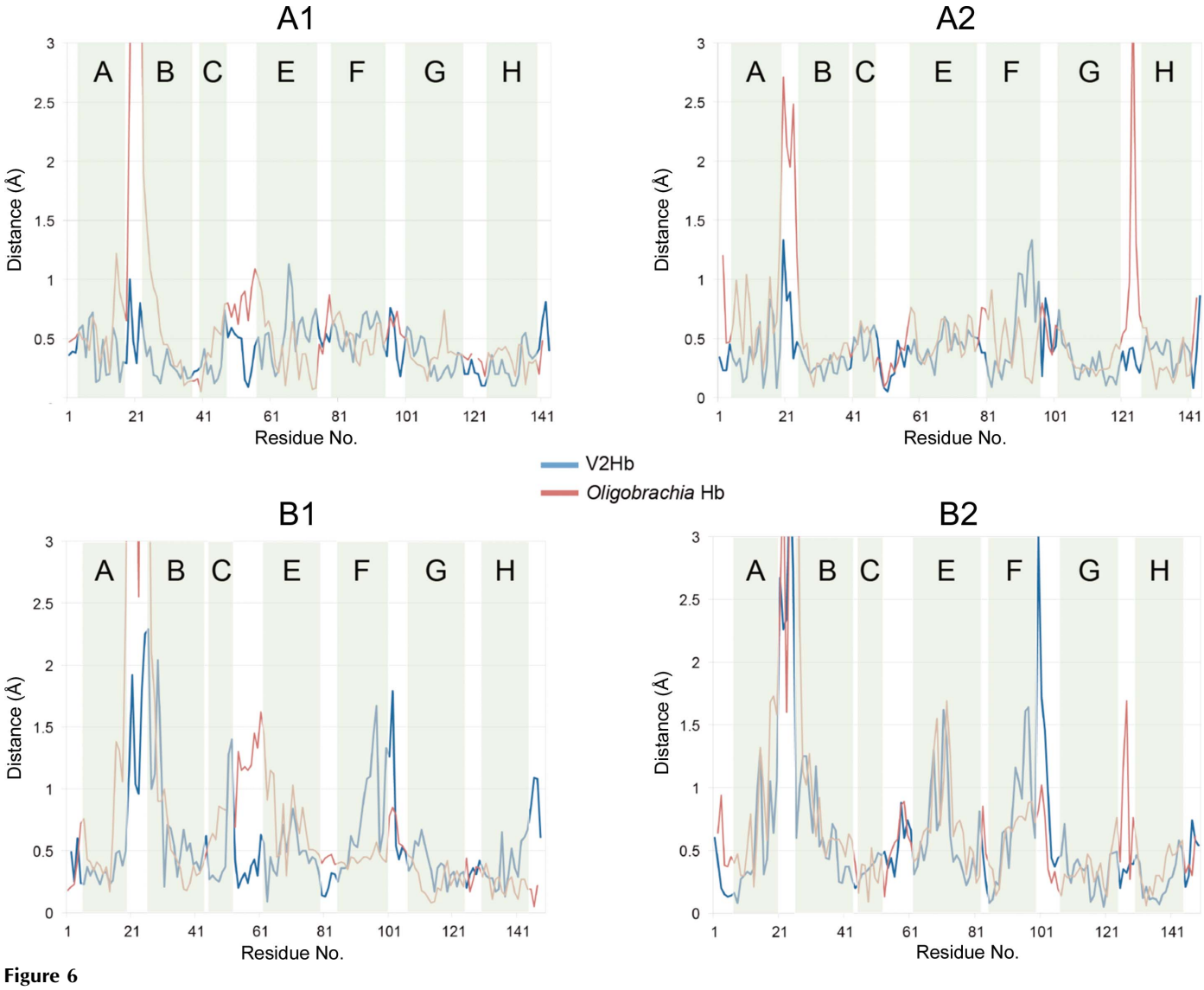

Figure 6
Distances of the C^{α}-atom positions between each subunit of oxy and deoxy V2Hb (blue) and those of *Oligobrachia* Hb (red). The helical regions of V2Hb are indicated by a light green background. The residues of *Oligobrachia* Hb are plotted using a structure-based alignment with V2Hb. The superpositions were performed using the whole 24-mer molecules to represent a combination of tertiary- and quaternary-structural changes.

binding causes a large movement of the GH loop, together with a slight movement around Asp55 at the neighbouring A2 subunit. Although the loop region just before the E helix of the B1 subunit moves significantly in *Oligobrachia* Hb, the corresponding region of V2Hb moves little because the glycosylation site is located in this region and a large movement of the carbohydrate chain would be restricted by the crystal packing. However, the restricted movement of this carbohydrate chain would have little effect on global structural changes between the oxy and deoxy structures in the crystal, because this loop region is distant from both the molecular twofold and threefold axes, and there are no direct interactions with the key moieties for the ternary-structural changes such as the AB loop and the E and F helices. Other remarkable differences are found in the AB loop regions and latter part of the F helices. These regions might be involved in the difference between the functions of the giant Hbs such as oxygen affinity and cooperativity.

Thus, because the structural changes of V2Hb between the oxy and deoxy states are quite similar to those of *Oligobrachia* Hb, it is strongly suggested that this manner of structural change is common among the 400 kDa giant Hbs. The space groups of the crystals of V2Hb and *Oligobrachia* Hb are $P6_3$ and $R32$, respectively. These facts clearly indicate that the contact regions for the symmetry mates of molecules are completely different from each other. Nonetheless, the conformations of the dimer and dodecamer subassembly of V2Hb and *Oligobrachia* Hb are almost the same in their oxy forms and also in their deoxy forms. The structural changes for the 24-meric whole molecule occur in the same fashion, thereby maintaining the molecular twofold and threefold axes of both of the giant Hbs. Therefore, we believe that these changes are not an artifact of the crystalline contacts, even though the large protrusion of the carbohydrate chain of V2Hb might restrict the local conformational change by the crystal packing, but would be the nature of structural changes between the oxy and deoxy states for all giant Hbs. Our findings based on the first deoxy structure of the 400 kDa Hb provides a first step towards a more accurate description of the cooperative mechanism of annelid giant Hbs.

NN and TN contributed equally to this work in performing the research. YF and KM contributed equally to this work in designing the research. We thank Dr J. Tsukahara of Kagoshima University and Mr K. Nakahata and Mrs N. Dewa of the 'Io World' Kagoshima City Aquarium for their cooperation with the tube-worm collection, transport and anatomical experiments. We thank the captain and crew of the training ship Nansei-maru of Kagoshima University and also thank the captain, crew and the ROV HyperDolphin operation team of the research vessel Natsushima of JAMSTEC for collecting the biological samples and data. We thank Drs K. Hasegawa, M. Kawamoto, H. Sakai, Y. Kawano, E. Yamashita and M. Yoshimura of SPring-8 for their help with the X-ray diffraction experiments. We also thank Dr T. Fujiwara of Shizuoka University for his help with the N-terminal amino-acid sequencing. This work was supported by a grant from the National Project on Protein Structural and Functional Analyses to KM and a Grant-in-Aid for Scientific Research on Priority Areas (16087205) to YF from the Ministry of Education, Culture, Sports, Science, and Technology of Japan.

References

Aki, Y., Nakagawa, T., Nagai, M., Sasayama, Y., Fukumori, Y. & Imai, K. (2007). *Biochem. Biophys. Res. Commun.* **360**, 673–678.
Brünger, A. T., Adams, P. D., Clore, G. M., DeLano, W. L., Gros, P., Grosse-Kunstleve, R. W., Jiang, J.-S., Kuszewski, J., Nilges, M., Pannu, N. S., Read, R. J., Rice, L. M., Simonson, T. & Warren, G. L. (1998). *Acta Cryst.* D**54**, 905–921.
Emsley, P., Lohkamp, B., Scott, W. G. & Cowtan, K. (2010). *Acta Cryst.* D**66**, 486–501.
Ewing, B., Hillier, L., Wendl, M. C. & Green, P. (1998). *Genome Res.* **8**, 175–185.
Flores, J. F., Fisher, C. R., Carney, S. L., Green, B. N., Freytag, J. K., Schaeffer, S. W. & Royer, W. E. Jr (2005). *Proc. Natl Acad. Sci. USA*, **102**, 2713–2718.
Fushitani, K., Imai, K. & Riggs, A. F. (1986). *J. Biol. Chem.* **261**, 8414–8423.
Laemmli, U. K. (1970). *Nature (London)*, **227**, 680–685.
Numoto, N., Nakagawa, T., Kita, A., Sasayama, Y., Fukumori, Y. & Miki, K. (2005). *Proc. Natl Acad. Sci. USA*, **102**, 14521–14526.
Numoto, N., Nakagawa, T., Kita, A., Sasayama, Y., Fukumori, Y. & Miki, K. (2008*a*). *Proteins*, **73**, 113–125.
Numoto, N., Nakagawa, T., Kita, A., Sasayama, Y., Fukumori, Y. & Miki, K. (2008*b*). *Biochemistry*, **47**, 11231–11238.
Otwinowski, Z. & Minor, W. (1997). *Methods Enzymol.* **276**, 307–326.
Perutz, M. F. (1968). *J. Cryst. Growth*, **2**, 54–56.
Royer, W. E. Jr, Knapp, J. E., Strand, K. & Heaslet, H. A. (2001). *Trends Biochem. Sci.* **26**, 297–304.
Schägger, H. & von Jagow, G. (1987). *Anal. Biochem.* **166**, 368–379.
Vagin, A. & Teplyakov, A. (2010). *Acta Cryst.* D**66**, 22–25.
Wang, J., Kamtekar, S., Berman, A. J. & Steitz, T. A. (2005). *Acta Cryst.* D**61**, 67–74.
Weber, R. E. & Vinogradov, S. N. (2001). *Physiol. Rev.* **81**, 569–628.
Winn, M. D. *et al.* (2011). *Acta Cryst.* D**67**, 235–242.